Influence of convection on the upper tropospheric O_3 and NO_x budget in southeastern China

Response to Anonymous Referee #3

Xin Zhang, Yan Yin, Ronald van der A, Henk Eskes, Jos van Geffen, Yunyao Li, Xiang Kuang, Jeff L. Lapierre, Kui Chen, Zhongxiu Zhen, Jianlin Hu, Chuan He, Jinghua Chen, Rulin Shi, Jun Zhang, Xingrong Ye, and Hao Chen

February 4, 2022

We thank the reviewer for his/her positive comments and very careful reading of our article. The individual corrections suggested are addressed below. The reviewer's comments will be shown in **red**, our response in **blue**, and changes made to the paper are shown in **black** block quotes. Unless otherwise indicated, page and line numbers correspond to the original manuscript. Figures, tables, or equations referenced as "Rn" are numbered within this response; if these are used in the changes to the paper, they will be replaced with the proper number in the revised version.

General Comments

(1) Since LNO_x is a key component of this study, affecting both O_3 chemistry and NO_2 and LNO_x air mass factors, it would be helpful to show several examples of WRF-Chem vertical profiles of these constituents for the two cases under different PE assumptions near and downwind of convection. For example, NO_2, LNO_2 and LNO_x profiles could be discussed in the context of the O_3 profiles of Fig. 4 and the ΔAMFs of Fig. 6. If feasible, it also would be interesting to compare the profiles with the standard profiles from TM5 used in the TROPOMI data product to illustrate the importance of local effects.

Thanks for your suggestions. We have added another short section to discuss the effects of LNO_x on O_3 profile using integrated reaction rate (IRR) results. Beside, the TM5, NO_2, LNO_2 and LNO_x profiles are also added to the supplement.

Impact of lightning NO_x on the O_3 profile

Furthermore, the IPR outputs including LNO emission are compared with these excluding LNO to explore the effects of LNO_x on O_3 (Table R1). The LNO_x reduces the net O_3 production by 25 % and 40 % during the convective period and life cycle of the 2019 case, respectively. The decreased chemistry contribution is less significant ($\leq$ 1%) for the 2020 case which has a smaller lightning density near the station. Note that the LNO_x can certainly enhance the downwind ozone production on the scale of days (Pickering et al., 1996; DeCaria et al., 2005). Therefore, it is necessary to estimate the LNO_x PE accurately (discussed later in Sect. 6.2).

Table R1 . Process analysis table for the mean O_3 integrated tendencies (10–14 km).

Period	Time	LNO (mol/flash)	advh + advz*	chem*	net*
Life Cycle	2019-07-25	0	-3.3 (-24.6 %)	16.7 (124.6 %)	13.4
	(03:20–05:40)	500	-2.3 (-28.8 %)	10.3 (128.8 %)	8.0
	2020-09-01	0	3.4 (9.6 %)	32.0 (90.4 %)	35.4
	(04:20–06:40)	500	4.4 (12.1 %)	31.9 (87.8 %)	36.3
Convective Period	2019-07-25	0	-19.6 (140.0 %)	5.6 (-40.0 %)	-14.0
	(04:20–05:00)	500	-20.0 (114.3 %)	2.5 (-14.3 %)	-17.5
	2020-09-01	0	-9.7 (-131.1 %)	17.1 (231.1 %)	7.4
	(05:40–06:20)	500	-10.1 (-148.5 %)	16.9 (248.5 %)	6.8

*The unit is 10^{10} molec. cm^{-3}. The percentage is the proportion of each part in the net O_3 change.

Additionally, the convection was divided into three regions by TROPOMI data: fresh lightning , downwind of fresh lightning, and aged lightning (See Sect. 6.1 and Fig. R5 for details). Firstly, the difference of O_3 (ΔO_3) profiles is obtained with different LNO PE assumption (Fig. R1a–c). In contrast with the net loss of ozone ($<$ 4 ppbv) over all height levels in Ott et al. (2007), the ΔO_3 is mostly positive ($<$ 1 ppbv) between 2 km and 5 km and negative ($>$ -3 ppbv) between 5 km and 12 km in our cases. The higher PE (700 mol/flash) slightly reduces the O_3 concentration by less than 1 ppbv at all levels compared with the default PE (500 mol/flash) and it even leads to negative ΔO_3 between 2 km and 5 km downwind of fresh lightning (Fig. R1b). The maximum O_3 loss is between 8 km and 10 km due to the peak of LNO_x (up to 2.6 ppbv) introduced in the model.

Then, the integrated reaction rate (IRR) is applied to determine the chemistry mechanism and the effect of LNO on the O_3 variation for two layers where the ΔO_3 is opposite: 800 hPa–500 hPa ($\Delta O_3 > 0$) and 500 hPa–200 hPa ($\Delta O_3 < 0$). The tropospheric O_3 is mainly controlled by five reaction rate terms (Pickering

et al., 1990; Bozem et al., 2014):

$$\frac{d}{dt}[\mathrm{O_3}] = k_1[\mathrm{NO}][\mathrm{HO_2}] + \sum_i k_i[\mathrm{NO}][\mathrm{R_iO_2}] - k_3[\mathrm{H_2O}][\mathrm{O(^1D)}] - k_4[\mathrm{HO_2}][\mathrm{O_3}] - k_5[\mathrm{OH}][\mathrm{O_3}] \quad \text{(R1)}$$

where k_i is the rate coefficient of the reaction between peroxy radicals (R_iO_2) and NO. The time series of each contribution to O_3 production are illustrated in Fig. R1d–i. Overall, the time series of IRR are more variable for the 2019 case due to the stronger activity as clarified in Sect. 4. The total net chemistry production of O_3 keeps positive for both layers. In detail, the reaction between NO and HO_2 always dominates the production while the oxidation of NO by RO_2 is about 40 %–60 % of that production. The dominant loss of O_3 is the photolysis (described by the reaction of $O(^1D)$ and H_2O) while the reaction between O_3 and OH is comparable during the convective period. The lowest contribution to O_3 loss, O_3 + HO_2 $\rightarrow$ OH + $2O_2$, is reduced during the convection because of the production of LNO, which captures the HO_2 reacting with O_3. Note that although the increase of total IRR induced by LNO_x can reach 1.36×10^7 molec. cm^{-3} s^{-1} and 2.60×10^6 molec. cm^{-3} s^{-1} in the low layer and high layer over these three regions, respectively, the net O_3 production actually decreases in the high layers (Fig. R1a–c) due to the combination of dynamic transport and chemical production related to LNO_x.

Relation between lightning and TROPOMI products

... Figure R4 shows that the AMF changes are mostly controlled by the LNO_x in the UT layer where the detection sensitivity is high (Beirle et al., 2009; Laughner and Cohen, 2017) and the LNO_x production reaches the peak (Fig. R2) ...

... The clouds are higher than 400 hPa ($p_{cloud} < 400$ hPa) and f_{effNO_2} is larger than 0.6 over fresh lightning pixels, but both aged lightning and downwind of fresh lightning areas have clouds lower than 400 hPa. This coincides with the mean cloud pressures in Fig. R2 and explains why UT $\Delta AMF_{trop} > 20$ % exits in Fig. R4b$_i$ and b$_{iii}$, indicating the possibility of LNO_x estimations over the aged lightning regions (Sect. 6.2). ...

... Besides, considering the region-specific LNO_x effects on AMFs, we need to include the representation of LNO_2 in the TROPOMI NO_2 retrievals better, especially outflow regions. The comparisons (Fig. R2) between the TROPOMI standard NO_2 profiles from TM5-MP and WRF-Chem also illustrate the importance of LNO_x, resolved convection transport, and emissions. Aircraft observations of NO and NO_2 will be useful to determine the exact roles (Laughner and Cohen, 2017).

(2) I find that giving the contributions of dynamic and chemical effects on O_3 as percentages is confusing (abstract, text and conclusions) when the percentages are greater than 100 and the effects have opposite signs. For example, to summarize the life cycles of both cases, it would be clearer to say that the chemistry increases O_3 in both cases and that the magnitude of the effect is 5–10 times the magnitude of dynamic effects (rather than using the > 87% figure).

Yes, the percentage changes are confusing. We have modified them according to your advice.

Abstract

... During the whole convection life cycle, the UT O_3 production is driven by the chemistry (5–10 times the magnitude of dynamic contribution) and reduced by the LNO_x (-40 %).

Convection impacts

... While the dynamic processes play an important role in the O_3 production, the positive chemistry contribution cannot be neglected in both cases and leads to the net increase in UT O_3 during the convective period of 2020 case. Specifically, the chemistry increases O_3 in both cases and the magnitude of the effect is 5–10 times that of dynamic effects. This demonstrates the dominant chemistry role in the overall effects of convection.

Conclusions

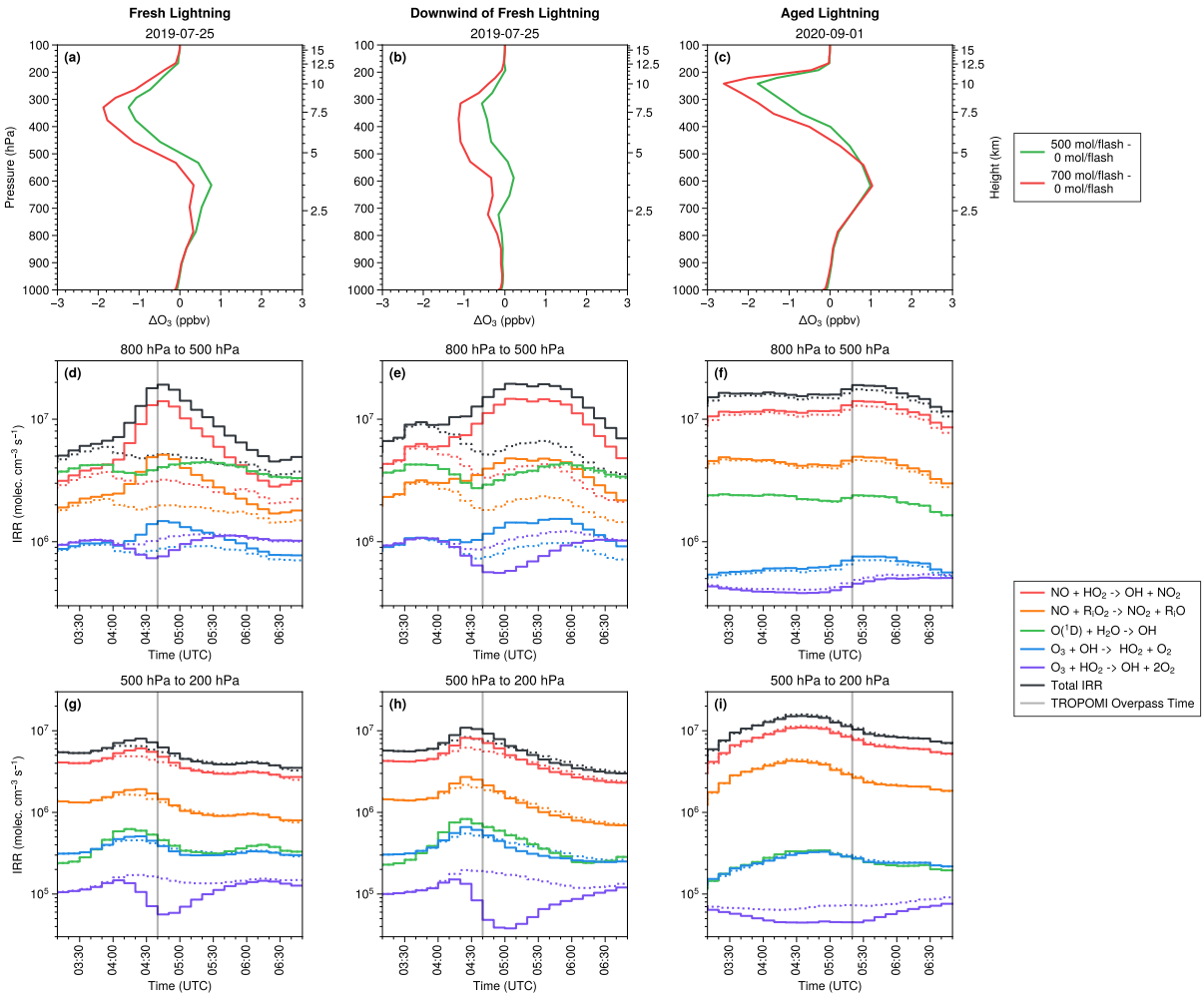

Figure R1 . (a–c) Changes in O_3 profiles due to LNO_x at TROPOMI overpass time in three regions (fresh lightning region, downwind of fresh lightning, and aged lightning area) as defined in Fig. 7. (d–f) Time series of the mean integrated reaction rate (IRR) between 800 hPa and 500 hPa. The legend shows detailed species and reactions. The Total IRR is the O_3 loss IRR subtracted from the O_3 production IRR (red and orange lines). The solid line shows the IRR with LNO (500 mol/flash) while the dashed line is without LNO. (g–i) Same as (d–f) but between 500 hPa and 200 hPa.

> ... The detailed analysis of integrated physical rates shows that the dynamic processes dominate the UT O_3 decrease during the convective stage of both cases. However, in the convection life cycle,the contribution of chemistry reactions to the UT O_3 production is 5–10 times that of dynamics.

(3) A substantial part of UT NO_2 seen in the 2020 event is likely not produced by the flashes counted in the region in the hour(s) immediately prior to overpass. As seen in Fig. 5a, b, increased SCD_{tropNO_2} is visible in regions where the cloud pressures are higher and cloud fractions are lower. This is mentioned in lines 210 – 215 on page 12 (the relevance of Fig. S5 to this should also be made clearer). Some estimate of ambient NO_2 is needed so that it can be subtracted as a tropospheric background before the LNO_x is computed. Studies have shown backgrounds can be substantial (e.g. Allen et al. 2019; Bucsela et al. 2019). A related issue is the relatively small estimate of 10% for the error introduced by the stratosphere (Allen et al.,

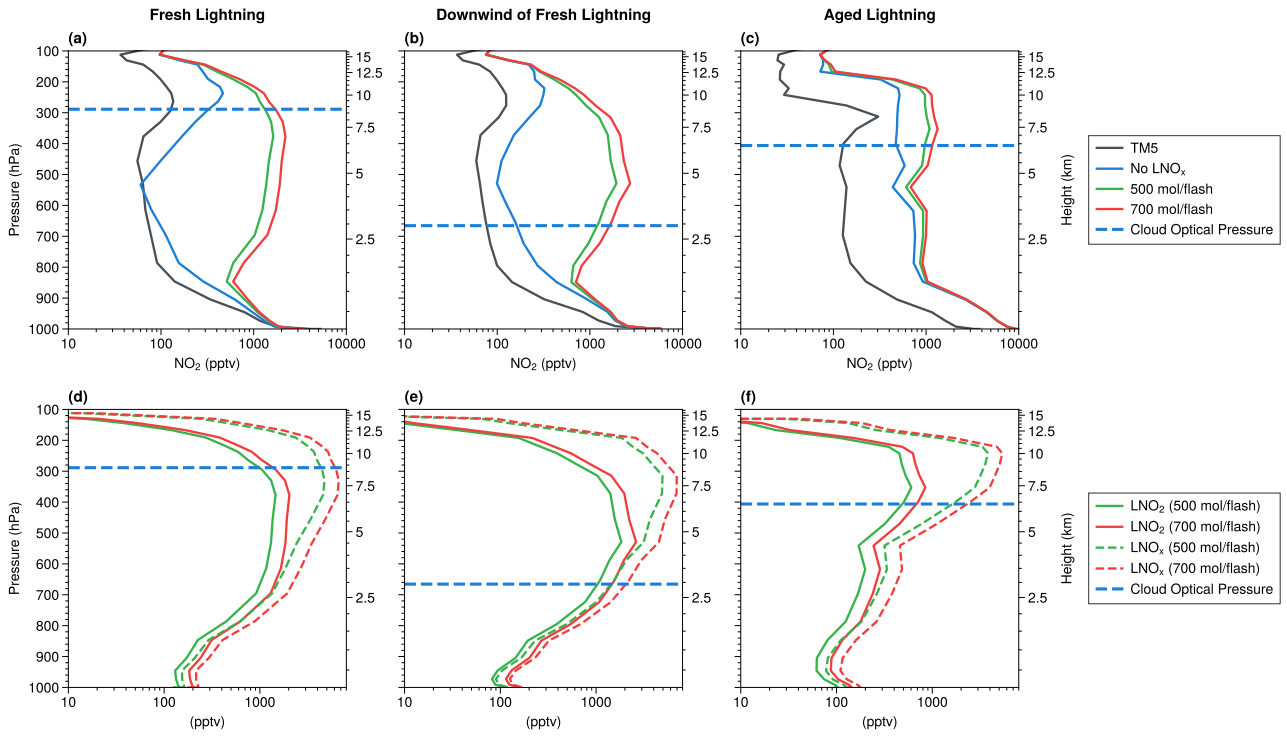

Figure R2 . Profiles with different lightning NO productions at TROPOMI overpass time over three regions (fresh lightning, downwind of fresh lightning, and aged lightning). (a–c) The NO_2 profiles compared with the official TM5 a priori NO_2 profile. (d–f) The lightning NO_2 and NO_x profiles. The blue dashed line is the cloud optical pressure detected by TROPOMI.

2019 - not 2021). This error assumed a tropospheric background subtraction that partially cancels stratospheric errors. Without this subtraction, the error would be larger.

1. Thanks, we have clarified the relevance of these figures for the ambient NO_2.
2. Note that the ambient NO_2 has been considered in the numerator of AMF_{LNO_x}:

$$AMF_{\mathrm{LNO}_x} = \frac{(1 - f_{effNO_2}) \int_{p_{surf}}^{p_{tp}} w_{clear}(p) NO_2(p)\, dp + f_{effNO_2} \int_{p_{cloud}}^{p_{tp}} w_{cloudy}(p) NO_2(p)\, dp}{\int_{p_{surf}}^{p_{tp}} LNO_x(p)\, dp} \quad \text{(R2)}$$

This is different from that of Pickering et al. (2016), Allen et al. (2019), and Bucsela et al. (2019). We have added the comparison in Sect. 2.3 (TROPOMI Data).

3. For the stratospheric errors, we have estimated the uncertainty as 9 % by applying a bias of $\pm\ 10^{14}$ molec. cm^2 (van Geffen et al., 2021). As mentioned in Bucsela et al. (2019), if they do not consider the background subtraction, "the stratospheric bias would have a >90 % effect on PE". Therefore, the low uncertainty (9 %) related to the stratospheric vertical column indicates that our AMF_{LNO_x} works well.

Relation between lightning and TROPOMI products

... Either the inadequate flash or weak convection could lead to a smaller SCD_{tropNO_2} over pixels with $f_{effNO_2} \approx 1$ because the TROPOMI can only see the LNO_2 above the clouds. In other words, the polluted NO_2 below the broken or thinner clouds is partially exposed if $f_{effNO_2} < 1$. The sensitivity tests of

the WRF-Chem a priori SCD_{tropNO_2} can help explain this phenomenon clearly (Fig. S5). The pixels of high SCD_{tropNO_2} with low cloud fraction belong to background NO_2 pollution (Fig. S5a and e), but the SCD_{tropNO_2} increased by UT LNO_2 is still visible compared with the lower SCD_{tropNO_2} without LNO_2 (Fig. S5b–d and f–h).

TROPOMI data

... In comparison with this study, Pickering et al. (2016), Allen et al. (2019), Bucsela et al. (2019), and Allen et al. (2021) defined another AMF_{LNO_x} to convert SCD_{tropNO_2} to the tropospheric NO_x vertical column density (VCD_{NO_x}). Then, their VCD_{LNO_x} can be calculated as 1) the slope of the regression between VCD_{NO_x} and flashes or 2) the VCD_{NO_x} subtracted by a tropospheric NO_x background. Because our AMF_{LNO_x} converts the SCD_{tropNO_2} to VCD_{LNO_x} directly, the additional estimation of background NO_2 is not needed for calculating LNO_x PE in Sect. 6.2.

Estimations of LNO_x

... Following Allen et al. (2019) and Zhang et al. (2020), the uncertainty of LNO_x is determined by LNO_x lifetime, lightning DE, NO/NO_2 ratio, LNO profile, and other sources (summarized in Table R2). The lifetime (τ) of NO_2 is replaced by 2 and 6 hours to evaluate the uncertainty as 27 % while another uncertainty is also 27 % related to lightning DE by changing the ratio of IC to CG to 2:1 and 4:1. The uncertainty caused by modeled NO/NO_2 ratios is assumed to be 30 % based on Allen et al. (2019) and the uncertainty related to LNO profile is 26 % by using the a priori NO_2 profile with 330 and 700 mol NO per flash. The uncertainty associated with the stratospheric vertical column is considered as 7 % by applying a bias of $\pm$ 10^{14} molec. cm^2 (van Geffen et al., 2021). The uncertainty caused by other possible error sources including systematic errors in slant columns, optical cloud pressure, and NO_2 redistributed by convection is difficult to quantify and assumed as 10 % following Allen et al. (2021). Assuming no correlation between errors, the total uncertainty (56 %) is estimated as the square root of the sum of the squares of all individual uncertainties. As a result, the LNO_x PE is 60 $\pm$ 33 mol NO_x per flash. It is less than that of our previous work (90 $\pm$ 50 mol NO_x per flash) over the continental United States (Zhang et al., 2020) and at the lower end of 120 $\pm$ 65 mol NO_x per flash obtained in Allen et al. (2021). Thus, more studies over China are necessary for the estimation of region-dependent LNO_x PEs.

Table R2 . Uncertainties for the estimation of LNO_x production efficiency.

Type	Uncertainty (%)
LNO_x lifetime	27 %
Lightning detection efficiency	27 %
NO/NO_2 ratio	30 %
LNO profile	26 %
Stratospheric vertical column	7 %
Others	10 %
Net	56 %

(4) Fig. 6 a_{ii} — c_{ii} and a_{iv} – c_{iv} show a decrease in AMF_{LNO_x} when LNO_x is enhanced at higher altitudes, in contrast to the behavior of AMF_{trop}, which is consistent with Fig. 7. Please include some words qualitatively discussing the behavior of AMF_{LNO_x}.

Added.

While the AMF_{LNO_x} **decreases by 5 %–40 %** for both cases, the changes of AMF_{trop} (ΔAMF_{trop}) are regionally specific and can be classified by the lightning activity: fresh lightning (MT $\Delta AMF_{trop} < -20$ %), downwind of fresh lightning (MT $\Delta AMF_{trop} > 20$ %), and aged lightning (UT $\Delta AMF_{trop} > 20$ %).

(5) In Figure 5f, why wasn't the northern part of the region included in the LNO_x analysis (section 5.2)? There appear to be adequate flashes there, along with LNO_x and a high cloud fraction. The southern/southeastern regions include areas of low cloud fraction that could potentially contaminate the measurements with anthropogenic NO_2. Also, if winds are from the WNW, shouldn't the flash-counting window be displaced WNW of the LNO_x window?

We had decided to include both parts in the analysis at the first time. However, there are many missing data in the northern convection. As replied in (3), the anthropogenic NO_2 has been included in the retrieval algorithm, which has also been applied in Zhang et al. (2020). We have fixed a bug of deriving the VCD_{LNO_x} and modified the selected region with clearer statements. The figure has been re-plotted and the LNO_x PE is estimated as 60 $\pm$ 33 mol NO_x per flash.

As the dissipated convection produced enough lightning and the UT winds within the storm were blowing from the west-northwest to east-southeast (Fig. R3a), the pattern of VCD_{LNO_x} can still be clearly identified (dashed rectangle in Fig. R3). Fortunately, there is a low VCD_{LNO_x} strip separating the northern and southern convection. With the careful selection, the LNO_x PE is estimated as 60 mol NO_x per flash. Although there are a few lightning flashes related to the VCD_{LNO_x} is outside of the region selection, it only affects the LNO_x PE by $\approx$ 2 mol, which is within the uncertainty discussed below.

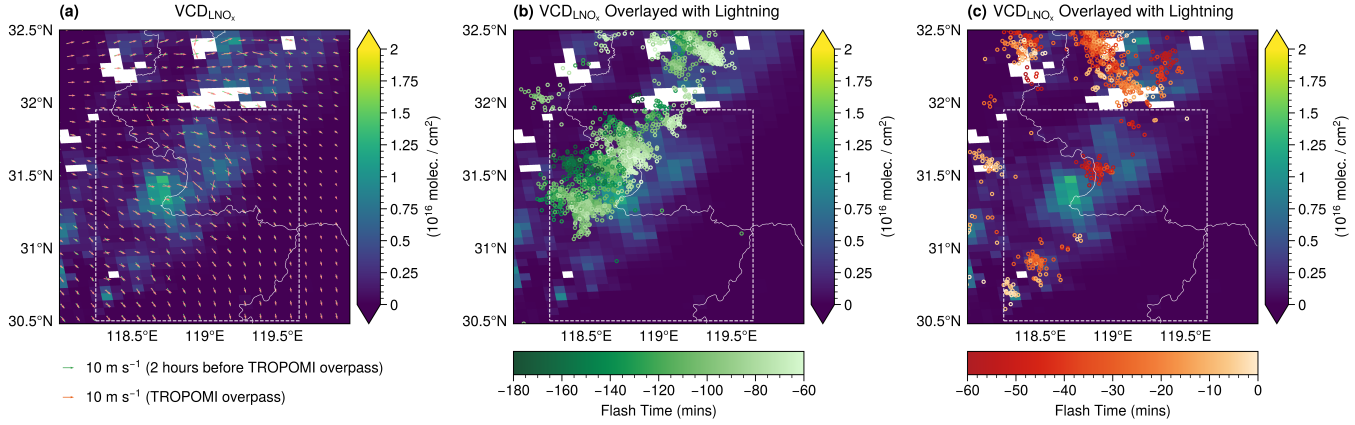

Figure R3 . The background is the distribution of LNO_x vertical column densities (VCD_{LNO_x}). The white rectangles are manually selected regions for the LNO_x PE estimation. The overlayed wind arrows in (a) are the 500 hPa horizontal wind simulated by WRF-Chem. The lightning dots in (b) and (c) are the flashes whose color depends on the occurring time relative to the TROPOMI overpass time.

Specific comments and technical corrections

1) Page 2, line 49: "We apply new a priori NO2..."

Thanks, fixed.

> We apply **new a priori NO_2** profiles into the retrieval algorithm to explore the sensitivity of AMFs to LNO_x.

2) Page 3, line 57: "...near the airmass convection that developed on 25..."

Fixed.

> Three Institute of Atmospheric Physics (IAP) ozonesondes had been launched near the airmass convection **that** developed on 25 July 2019.

3) Page 3, line 64: "...the observed difference of more than 65%."

Fixed.

> therefore the daily variation cannot explain the observed difference of **more than 65 %**.

4) Page 5, line 84: "...with a constant IC/CG ratio of 3:1 based on Wu et al..."

Fixed.

> Because the IC DE of all these lightning data is low in China, we conservatively used the merged CG data **with a constant IC/CG ratio of 3:1 based on** ...

5) Page 5, lines 81 – 85: Please add some detail on how the 3 datasets were merged. Was CNDLN used to estimate a DE for ENTLN and WWLLN?

Added.

> The detection efficiency (DE) of cloud-to-ground (CG) flashes is about 90 % for the CNLDN data in Jiangsu province (Li et al., 2017) while ENTLN and WWLLN detect both intro-cloud (IC) and CG flashes with specific detection frequency (1 Hz–12 MHz for ENTLN and 3–30 kHz for WWLLN). In the ENTLN data, groups of pulses are classified as a flash if they are within 700 ms and 10 km. Both strokes and lightning flashes composed of one or more strokes are included in the preprocessed data obtained from the ENTLN. The detailed processing algorithm of the WWLLN is given by Rodger et al. (2004). The WWLLN strokes and pulses are combined with ENTLN into one dataset (ENGLN) within 10 km and 0.7 s as mentioned in Virts and Goodman (2020). **To increase the lightning data coverage in our study, the CG flashes of ENGLN and CNLDN datasets are combined using spatial and temporal clustering criteria of 10 km and 0.5 s (Zhao et al., 2020). Although CG detection efficiency of ENGLN is not known for this region due to a lack of validation data, merging these three datasets should provide a sufficiently high CG flash detection efficiency for this analysis. Because the IC DE of all these lightning data is low in China, we conservatively use the merged CG data with a constant IC/CG ratio of 3:1 based on Wu et al. (2016) and Bandholnopparat et al. (2020). IC data will become more accurate if more Chinese total lightning networks, such as Beijing Lightning Network (BLNET; Srivastava et al., 2017), are available**.

6) Page 6, line 105: Please add a similar equation for AMF_{trop}, since it is used in section 5.1.

Added.

We replaced the tropospheric AMF (AMF_{trop}) with a new AMF called AMF for LNO_x (AMF_{LNO_x}) to derive the tropospheric LNO_x vertical column density (VCD_{LNO_x}). The concept of AMF_{LNO_x} inherits from the AMF_{trop} derived by a function of several parameters (solar zenith angle, viewing zenith angle, relative azimuth angle, surface albedo, surface pressure, cloud fraction, cloud height, and a priori trace gas profile). Briefly, the numerator is the modeled tropospheric NO_2 slant column density (SCD_{tropNO_2}) and the denominator is the modeled VCD (VCD_{NO_2} or VCD_{LNO_x}). In detail, these two AMFs can be calculated as:

$$AMF_{\text{Trop}} = \frac{(1 - f_{effNO_2}) \int_{p_{surf}}^{p_{tp}} w_{clear}(p) NO_2(p)\, dp + f_{effNO_2} \int_{p_{cloud}}^{p_{tp}} w_{cloudy}(p) NO_2(p)\, dp}{\int_{p_{surf}}^{p_{tp}} NO_2(p)\, dp}$$

$$AMF_{\text{LNO}_x} = \frac{(1 - f_{effNO_2}) \int_{p_{surf}}^{p_{tp}} w_{clear}(p) NO_2(p)\, dp + f_{effNO_2} \int_{p_{cloud}}^{p_{tp}} w_{cloudy}(p) NO_2(p)\, dp}{\int_{p_{surf}}^{p_{tp}} LNO_x(p)\, dp}$$

7) Page 7, line 161: "The squall line on 1 September, 2020 was born..."

Sorry for the wrong date. Fixed.

The squall line on **1 September, 2020** was born in the ...

8) Page 10, Fig. 4 caption: "The vertical distributions of the O3 net production rate and tendency..."

Fixed.

The vertical distributions of the O_3 **net production rate and tendency** due to ...

9) Page 10, line 198: Regarding "...less significant (< 1%)..." From Table 1, I estimate that for the 2020 case, changes in chemistry affect net O3 production by 0.3% and ≈3% during the life cycle and convective period, resp.

The changes are (16.9-17.1)/17.1 = 1% and (31.9-32.0)/32.0 = 0.3% for the convective period and life cycle, resp (Table R1).

The decreased chemistry contribution is less significant **($\leq$ 1%)** for the 2020 case which has a smaller lightning density near the station.

10) P10, line 201: "...can certainly enhance the downwind ozone production on the scale of days..."

Fixed.

Note that the LNO_x can certainly enhance the downwind ozone production **on the scale of days** (Pickering et al., 1996; DeCaria et al., 2005).

11) Page 12, Fig. 5 caption: Please state white grid cells are for missing TROPOMI data (no2_scd_flag > 0 ?).

We have modified the caption and added the definition of no2_scd_flag in the Appendix A.

Fig caption

... These white grid cells stand for missing TROPOMI data (no2_scd_flag $\neq 0$), as defined in Appendix A.

Appendix A: Flag definitions used in this study

The no2_scd_flag is introduced to make usage of the NO_2 slant column (SCD) data easier, by gathering information from a few variables into one flag (Table R3). This flag can thus be used for filtering, though with care as it probably does not cover all possible situation. Here "δ" refers to the SCD error (in mol/m^2) and "pqf" stands for processing quality flag.

Table R3 . Definition of no2_scd_flag.

Value	Meaning
-1	no SCD value due to saturation limit exceeded, i.e. pqf=54
0	SCD with $\delta < 3.3\times10^{-5}$ & no error reported
1	SCD with $\delta < 3.3\times10^{-5}$ & error reported: pqf=55
2	SCD with $\delta < 3.3\times10^{-5}$ & other error reported, e.g. pqf=41
3	SCD with $\delta \geq 3.3\times10^{-5}$ & no error reported
4	SCD with $\delta \geq 3.3\times10^{-5}$ & error reported: pqf=55
5	SCD with $\delta \geq 3.3\times10^{-5}$ & other error reported, e.g. pqf=41
FillValue	no SCD due other error (prior to the Differential Optical Absorption Spectroscopy fit)

12) Page 13, lines 218-219: "... middle troposphere (MT, 800 hPa to 400 hPa), upper troposphere (UT 400 hPa to 150 hPa)..."

Added the abbreviation of upper troposphere.

The changes in the retrieved AMFs are examined by replacing profiles in three tropospheric layers independently: middle troposphere (MT, 800 hPa to 400 hPa), upper troposphere (**UT**, 400 hPa to 150 hPa), and troposphere (surface to tropopause)

13) Page 13, line 220-221: "...Figure 6 shows that the AMF changes...". Also, Beirle et al. (2009) noted a decrease in sensitivity in the UT due to the NO2/NOx branching ratio.

Added.

Figure 7 shows that the **AMF** changes are mostly controlled by the LNO_x in the UT layer where the detection sensitivity is high **(Beirle et al., 2009; Laughner and Cohen, 2017) and the LNO_x production reaches the peak (Fig. S6)**.

14) Page 13, line 226: "...UT ΔAMFtrop > 20 % exists in Fig. 6bi and biii,"

Fixed.

This explains why UT $\Delta AMF_{trop} > 20$ % exits in Fig. 7b$_i$ and b$_{iii}$,

15) Page 14, Fig 6 caption:
"...is the AMF_{trop} with 500 mol NO per flash relative to 0 mol NO per flash"
"...is the AMF_{LNO_x} with 700 mol NO per flash relative to 500 mol NO per flash"
Also, it would help to see the ovals overplotted on all figures for easier comparison.

Thanks for the suggestion. We have added ovals to the first and third row of Fig. R4, because the ΔAMF_{LNO_x} is mostly negative and the figure is cleaner than that full of ovals.

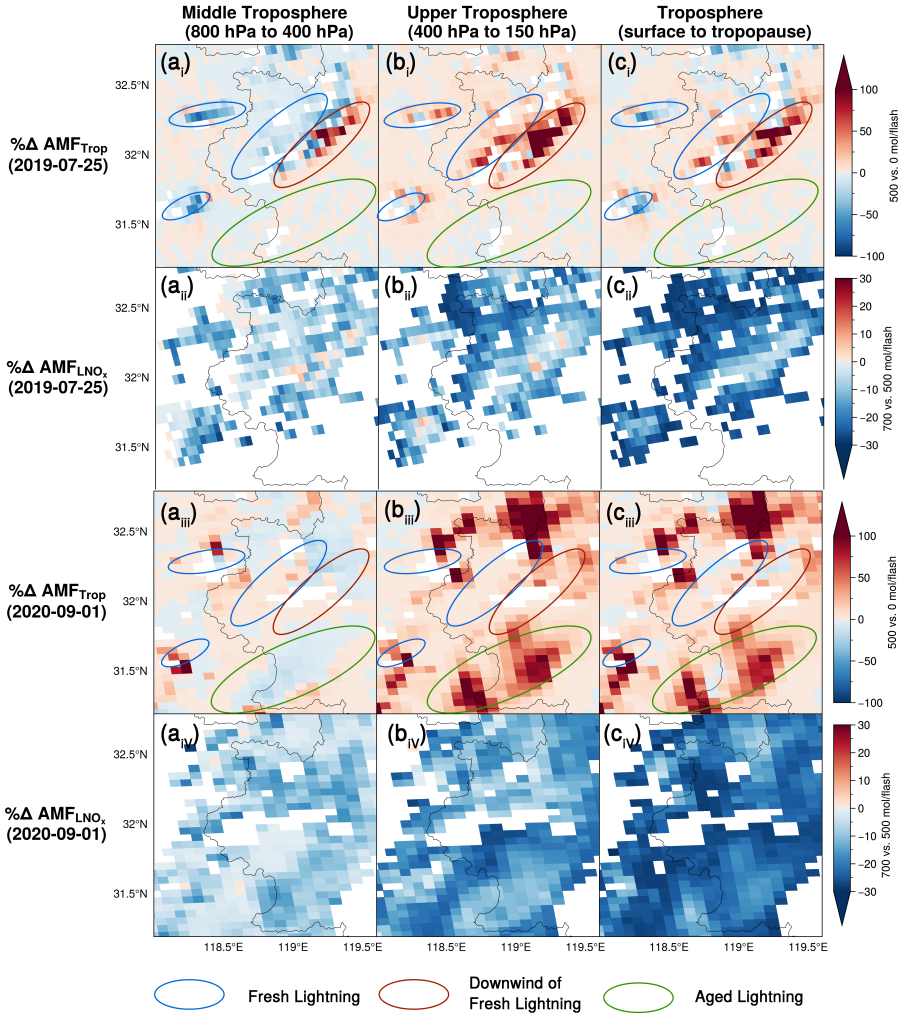

Figure R4 . The percent differences of AMFs by replacing the a priori NO_2 profiles at three layers: middle troposphere (left), upper troposphere (middle), and troposphere (right). ΔAMF_{trop} is the comparison of the AMF_{trop} with 500 mol NO per flash relative to 0 mol NO per flash. ΔAMF_{LNO_x} is the comparison of the AMF_{LNO_x} with 700 mol NO per flash relative to 500 mol NO per flash. Three regions are annotated: fresh lightning (blue), downwind of fresh lightning (red), and aged lightning (green). Because of the quite large AMF_{LNO_x} values in pixels with little lightning, ΔAMF_{LNO_x} is shown over pixels where $0 < AMF_{LNO_x} < 10$.

16) Page 15, Fig 7: Please label the x-axes in (b), (c) and (d).

Added (Fig. R5).

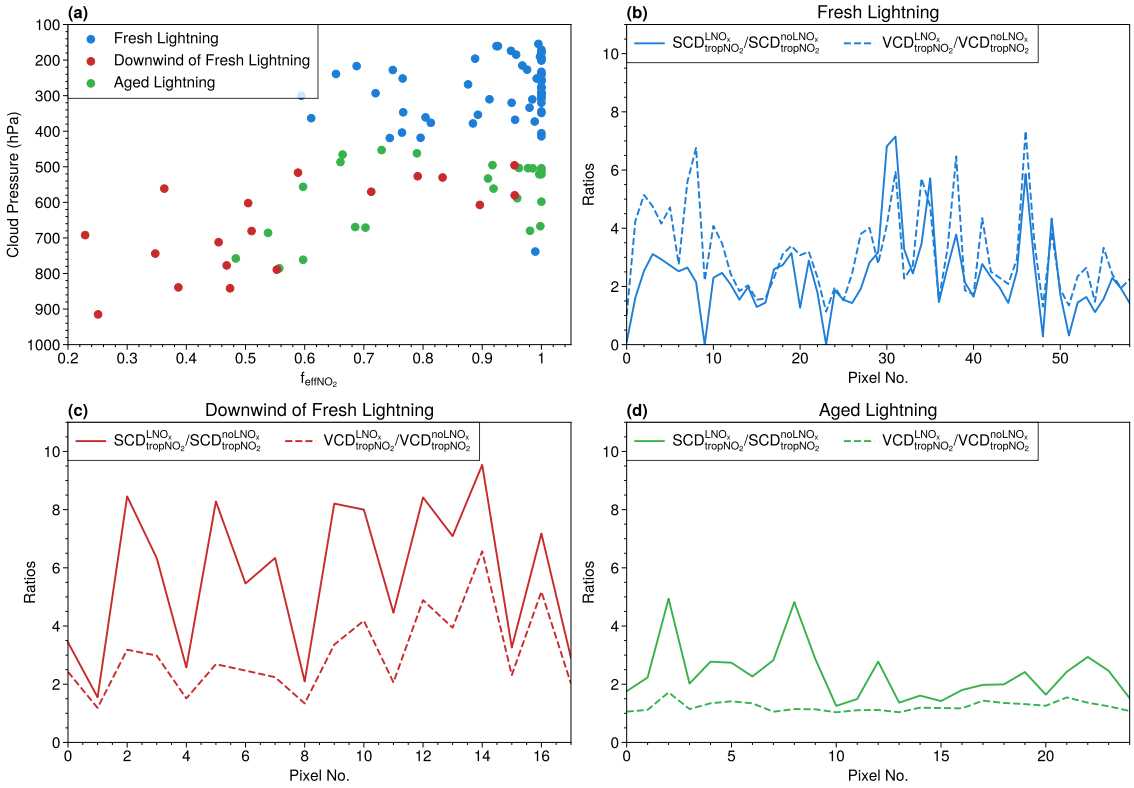

Figure R5 . (a) The relationship between cloud pressure and f_{effNO_2} for three regions defined in Fig. 7: fresh lightning region, downwind of fresh lightning, and aged lightning area. (b–d) The a priori $SCD^{LNO_x}_{tropNO_2}/SCD^{noLNO_x}_{tropNO_2}$ and a priori $VCD^{LNO_x}_{tropNO_2}/VCD^{noLNO_x}_{tropNO_2}$ of pixels in these three regions. The LNO_x superscript indicates that the a priori variable is calculated with LNO_x (500 mol NO per flash) and the $noLNO_x$ superscript is without LNO_x.

17) Figure S1, caption: "... WRF-Chem simulations for the 2019 and 2020 cases."

Fixed.

Domain and terrain height (m) of the WRF-Chem simulations for the 2019 and 2020 cases.

18) Figure S2: The times/dates in the legend of (a) are not correct

Sorry for the misleading. Because the time resolution of WACCM is 6 hours, the time shown in the legend (Fig. R6) is different from that of ozonesonde.

19) Figure S3, caption: "... in Fig. 2 for 25 July, 2019.""

Fixed (Fig. R7).

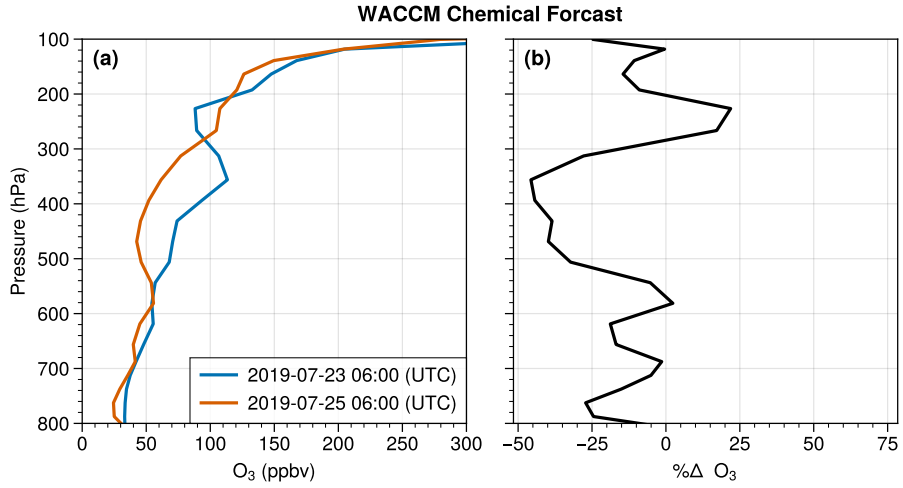

Figure R6 . (a) Regional mean (118.5°E – 119.5°E, 31.5°N – 32.5°N) preconvection (blue) and postconvection (orange) O_3 profiles from the **6-hour** WACCM forecasts. (b) The percent difference of O_3 profiles in (a).

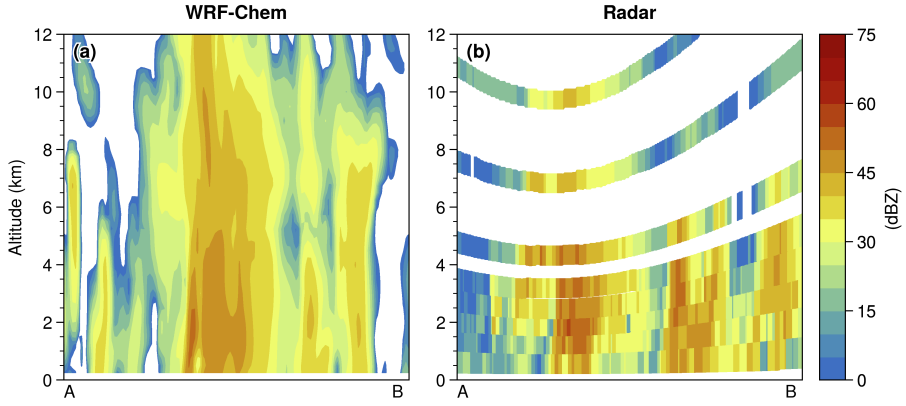

Figure R7 . Vertical cross sections of (a) WRF-Chem simulated and (b) observed radar reflectivity fields along the transect lines (AB) in Fig. 2 **for 25 July, 2019**.

References

Allen, D. J., Pickering, K. E., Bucsela, E., Krotkov, N., and Holzworth, R.: Lightning NO_x Production in the Tropics as Determined Using OMI NO_2 Retrievals and WWLLN Stroke Data, J. Geophys. Res. Atmos., 124, 13 498–13 518, https://doi.org/10.1029/2018JD029824, 2019.

Allen, D. J., Pickering, K. E., Bucsela, E., Geffen, J. V., Lapierre, J., Koshak, W., and Eskes, H.: Observations of Lightning NO_x Production from TROPOMI Case Studies over the United States, J. Geophys. Res. Atmos., 126, e2020JD034 174, https://doi.org/10.1029/2020JD034174, 2021.

Bandholnopparat, K., Sato, M., Adachi, T., Ushio, T., and Takahashi, Y.: Estimation of the IC to CG Ratio Using JEM-GLIMS and Ground-Based Lightning Network Data, J. Geophys. Res. Atmos., 125, e2019JD032 195, https://doi.org/10.1029/2019jd032195, 2020.

Beirle, S., Salzmann, M., Lawrence, M. G., and Wagner, T.: Sensitivity of Satellite Observations for Freshly Produced Lightning NO_x, Atmos. Chem. Phys., 9, 1077–1094, https://doi.org/10.5194/acp-9-1077-2009, 2009.

Bozem, H., Fischer, H., Gurk, C., Schiller, C. L., Parchatka, U., Koenigstedt, R., Stickler, A., Martinez, M., Harder, H., Kubistin, D., Williams, J., Eerdekens, G., and Lelieveld, J.: Influence of Corona Discharge on the Ozone Budget in the Tropical Free Troposphere: A Case Study of Deep Convection during GABRIEL, Atmos. Chem. Phys., 14, 8917–8931, https://doi.org/10.5194/acp-14-8917-2014, 2014.

Bucsela, E., Pickering, K. E., Allen, D., Holzworth, R., and Krotkov, N.: Midlatitude Lightning NO_x Production Efficiency Inferred from OMI and WWLLN Data, J. Geophys. Res. Atmos., 124, 13 475–13 497, https://doi.org/10.1029/2019jd030561, 2019.

DeCaria, A. J., Pickering, K. E., Stenchikov, G. L., and Ott, L. E.: Lightning-Generated NO_x and Its Impact on Tropospheric Ozone Production: A Three-Dimensional Modeling Study of a Stratosphere-Troposphere Experiment: Radiation, Aerosols and Ozone (STERAO-A) Thunderstorm, J. Geophys. Res. Atmos., 110, https://doi.org/10.1029/2004JD005556, 2005.

Laughner, J. L. and Cohen, R. C.: Quantification of the Effect of Modeled Lightning NO_2 on UV–Visible Air Mass Factors, Atmos. Meas. Tech., 10, 4403–4419, https://doi.org/10.5194/amt-10-4403-2017, 2017.

Li, F., Wu, L., and Li, Y.: Lightning Data Analysis of the CMA Network in China, Atmos. Meas. Tech. Discuss., pp. 1–22, https://doi.org/10.5194/amt-2016-380, 2017.

Ott, L. E., Pickering, K. E., Stenchikov, G. L., Huntrieser, H., and Schumann, U.: Effects of Lightning NO_x Production during the 21 July European Lightning Nitrogen Oxides Project Storm Studied with a Three-Dimensional Cloud-Scale Chemical Transport Model, J. Geophys. Res. Atmos., 112, 61, https://doi.org/10.1029/2006JD007365, 2007.

Pickering, K. E., Thompson, A. M., Dickerson, R. R., Luke, W. T., McNamara, D. P., Greenberg, J. P., and Zimmerman, P. R.: Model Calculations of Tropospheric Ozone Production Potential Following Observed Convective Events, J. Geophys. Res., 95, 14 049, https://doi.org/10.1029/JD095iD09p14049, 1990.

Pickering, K. E., Thompson, A. M., Wang, Y., Tao, W.-K., McNamara, D. P., Kirchhoff, V. W. J. H., Heikes, B. G., Sachse, G. W., Bradshaw, J. D., Gregory, G. L., and Blake, D. R.: Convective Transport of Biomass Burning Emissions over Brazil during TRACE A, J. Geophys. Res., 101, 23 993–24 012, https://doi.org/10.1029/96JD00346, 1996.

Pickering, K. E., Bucsela, E., Allen, D., Ring, A., Holzworth, R., and Krotkov, N.: Estimates of Lightning NO_x Production Based on OMI NO_2 Observations over the Gulf of Mexico, J. Geophys. Res. Atmos., 121, 8668–8691, https://doi.org/10.1002/2015JD024179, 2016.

Rodger, C. J., Brundell, J. B., Dowden, R. L., and Thomson, N. R.: Location Accuracy of Long Distance VLF Lightning Locationnetwork, Ann. Geophys., 22, 747–758, https://doi.org/10.5194/angeo-22-747-2004, 2004.

Srivastava, A., Tian, Y., Qie, X., Wang, D., Sun, Z., Yuan, S., Wang, Y., Chen, Z., Xu, W., Zhang, H., Jiang, R., and Su, D.: Performance Assessment of Beijing Lightning Network (BLNET) and Comparison with Other Lightning Location Networks across Beijing, Atmospheric Research, 197, 76–83, https://doi.org/10.1016/j.atmosres.2017.06.026, 2017.

van Geffen, J., Eskes, H., Compernolle, S., Pinardi, G., Verhoelst, T., Lambert, J.-C., Sneep, M., ter Linden, M., Ludewig, A., Boersma, K. F., and Veefkind, J. P.: Sentinel-5P TROPOMI NO_2 Retrieval: Impact of Version v2.2 Improvements and Comparisons with OMI and Ground-Based Data, Atmospheric Measurement Techniques Discussions, pp. 1–37, https://doi.org/10.5194/amt-2021-329, 2021.

Virts, K. S. and Goodman, S. J.: Prolific Lightning and Thunderstorm Initiation over the Lake Victoria Basin in East Africa, Mon. Wea. Rev., 148, 1971–1985, https://doi.org/10.1175/MWR-D-19-0260.1, 2020.

Wu, F., Cui, X., Zhang, D.-L., Liu, D., and Zheng, D.: SAFIR-3000 Lightning Statistics over the Beijing Metropolitan Region during 2005–07, J. Appl. Meteorol. Climatol., 55, 2613–2633, https://doi.org/10.1175/jamc-d-16-0030.1, 2016.

Zhang, X., Yin, Y., van der A, R., Lapierre, J. L., Chen, Q., Kuang, X., Yan, S., Chen, J., He, C., and Shi, R.: Estimates of Lightning NO_x Production Based on High-Resolution OMI NO_2 Retrievals over the Continental US, Atmos. Meas. Tech., 13, 1709–1734, https://doi.org/10.5194/amt-13-1709-2020, 2020.

Zhao, P., Li, Z., Xiao, H., Wu, F., Zheng, Y., Cribb, M. C., Jin, X., and Zhou, Y.: Distinct Aerosol Effects on Cloud-to-Ground Lightning in the Plateau and Basin Regions of Sichuan, Southwest China, Atmos. Chem. Phys., 20, 13 379–13 397, https://doi.org/10.5194/acp-20-13379-2020, 2020.